Applied Surface Science 270 (2013) 722–727

Contents lists available at SciVerse ScienceDirect

Applied Surface Science

journal homepage: www.elsevier.com/locate/apsusc

Core–shell heterostructures of SnM (M = (Fe, Ni, and Cr) or Cu) alloy nanowires @ CNTs on metallic substrates

Yu Zhong[a], Yong Zhang[a], Mei Cai[b], Michael P. Balogh[b], Ruying Li[a], Xueliang Sun[a,*]

[a] Department of Mechanical and Materials Engineering, University of Western Ontario, London, Ontario, N6A 5B9, Canada
[b] General Motors Research and Development Center, Warren, MI 48090-9055, United States

ARTICLE INFO

Article history:
Received 15 January 2013
Accepted 20 January 2013
Available online 28 January 2013

Keywords:
Core–shell structure
Alloy nanowires
Metallic substrates

ABSTRACT

Sn alloy nanowires encapsulated in carbon nanotubes (SnM (M = (Fe, Ni, and Cr) or Cu) @ CNTs) were prepared in situ by a chemical vapor deposition (CVD) method, in which Sn came from a vaporized precursor while the alloy elements were supplied by the substrate. The heterostructures were grown on two types of substrates including stainless steel with high catalytic effectiveness and Cu substrates with low catalytic effectiveness for generating graphite layers, respectively. Pure Sn powder and C_2H_4 were employed to provide Sn and carbon precursors. The products were investigated by scanning electron microscopy (SEM), high resolution transmission electron microscopy (HRTEM) and scanning transmission electron microscopy–energy dispersive X-ray spectroscopy (STEM–EDS) mapping. The morphology, structure and composition of the nanomaterials depended significantly on the surface conditions of the substrates. While SnCu alloy nanowires encapsulated in carbon nanotubes were grown on the Cu substrate, carbon nanotubes filled with alloy nanowires and porous carbon fibers decorated internally with alloy particles were observed on the stainless steel substrate. The growth mechanisms of the heterostructures were proposed.

1. Introduction

One-dimensional (1D) nanomaterials have attracted intensive research interest due to their unique structures and distinct physical and chemical properties [1–8]. These 1D nanomaterials are considered as promising candidates for various applications such as sensors [9–11], field emission [12], scanning probe tips [13] and building blocks in electric devices [14].

To approach high performance nanodevices, 1D nanomaterials with complex architectures have been developed, in which coaxial core–shell heterostructures have attracted particular interest due to their distinct combination of core and shell structure promising broader device applications. Carbon layers are popularly used to form a thin shell which can increase the conductivity of the composites, buffer the volume change and avoid aggregation of metal nanowires [15,16]. On the other hand, tailoring pristine nanomaterials by incorporating different materials is also employed to yield improved properties for many applications [17–19]. Singh et al. produced Zn-doped In_2O_3 nanowires as gas sensor [20]. Gao et al. prepared Cu-doped ZnO nanowires with enhanced ferromagnetism [21].

Sn-based nanostructures are of special interest because of their potential applications in the Li-ion batteries [22–24] and superconductors [25]. Recently, Sn-based 1D heterostructures have been widely explored. Li et al. prepared Sn nanowires encapsulated inside the carbon nanotubes (Sn@CNTs) by an in situ chemical vapor deposition (CVD) method [15], and their potential as fuel cell electrodes was investigated as well [26]. Ragan et al. prepared nonlithographic epitaxial SnGe dense nanowires arrays for optoelectronic applications [27]. However, the heterostructure of SnM (M = transitional metals) alloy nanowires encapsulated in carbon nanotubes has rarely been investigated.

In this paper, in order to yield the novel nanostructure by combining coating and alloying, we report the in situ growth of Sn-alloy nanomaterials encapsulated in carbon nanotubes core–shell heterostructures (Sn-alloy@CNTs) by feeding Sn from a vaporized precursor and alloy elements from the substrate, respectively, in a CVD process. In this method, the products were directly deposited on the stainless steel and Cu substrates acting as both the donors of alloy elements and the supporting substrates. The effects of the stainless steel and Cu substrates on the growth morphology and structure of the products were investigated.

2. Materials and methods

The Sn-alloy@CNTs heterostructures were synthesized by a CVD method. Sn powder (melting point: 231 °C) was chosen as the

* Corresponding author. Tel.: +1 519 6612111x87759; fax: +1 519 6613020.
E-mail address: xsun@eng.uwo.ca (X. Sun).

0169-4332/$ – see front matter © 2013 Elsevier B.V. All rights reserved.
http://dx.doi.org/10.1016/j.apsusc.2013.01.138

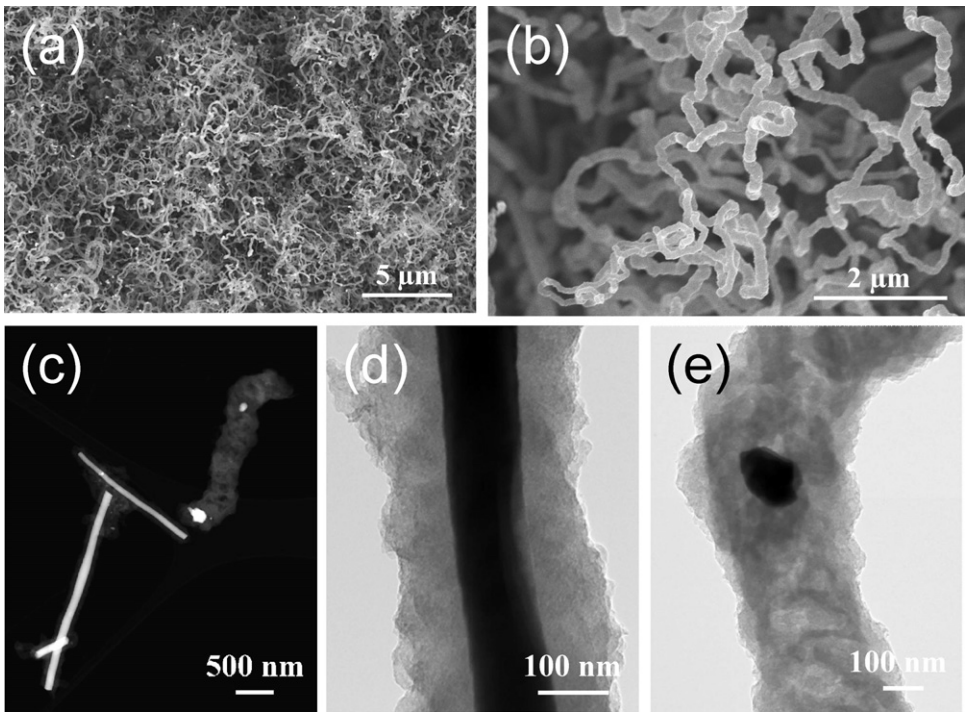

Fig. 1. (a and b) SEM images of heterostructures on stainless steel. (c) HAADF analysis presenting two types of nanostructures: (d) hollow tube filled by solid nanowire (HT) and (e) porous fiber decorated internally with nanoparticles (PF).

starting material and loaded in a ceramic boat. The ceramic boat was put in the center of a quartz tube mounted in a tube furnace. The substrates (stainless steel 304 and pure Cu) were placed aside the Sn powder at the down stream of an Ar flow (400 sccm) which was used as a carrier gas. The pre-treatment was applied to the substrates. Firstly, the substrates were polished by sand paper; secondly, the surface of the substrates was etched by HCl (1 mol/L) for 30 min; finally, the substrates were washed with distilled water and dried. Before the synthesis started, air in the tube was purged by the Ar flow for 15 min. When the furnace was heated up to the required temperatures (stainless steel: 900 °C, Cu: 850 °C), hydrocarbon gas (C_2H_4: 5 sccm) was introduced into the reaction zone to initiate the reaction. Then the growth of heterostructures occurred at the surface of the substrates. The reaction conditions were maintained for 2 hours, and then power of the furnace was switched off and cooled down to room temperature.

The products were characterized by using field emission scanning electron microscopy (FE-SEM, Hitachi 4800S SEM) and transmission electron microscopy (TEM, Hitachi 7000) and high resolution transmission electron microscopy (HRTEM, JEOL 2010 aberation corrected FEG) equipped with an energy dispersive x-ray spectrometer (EDS) capable of collecting EDS-scanning transmission electron microscopy (STEM) data and EDS-STEM maps.

3. Results and discussion

3.1. Stainless steel substrate

Fig. 1a and b show the SEM images of the nanostructures growing on the stainless steel substrate at 900 °C. After reaction, the surface of the substrate was completely covered by dense products with 1D nanowire-like morphology. The diameter of the products ranges from 150 to 300 nm. High-angle annular dark-field (HAADF) STEM image (Fig. 1c) reveals that the products have two types of nanostructures and both of them possess core–shell structure: one is hollow tubes filled by solid nanowires (HT) (Fig. 1d), and the other is porous fibers internally decorated with nanoparticles (PF) (Fig. 1e).

The details of these nanostructures were investigated by HRTEM. Fig. 2 shows the HRTEM images of the HT nanostructure which has the typical core–shell structure comprising two parts: CNT as the outer shell and metal nanowire as the inner solid core. The CNT has a straight tubular cavity filled by a solid metal nanowire, and rough outer surface. The average thickness of the outer carbon shell is around 80 nm, while the average diameter

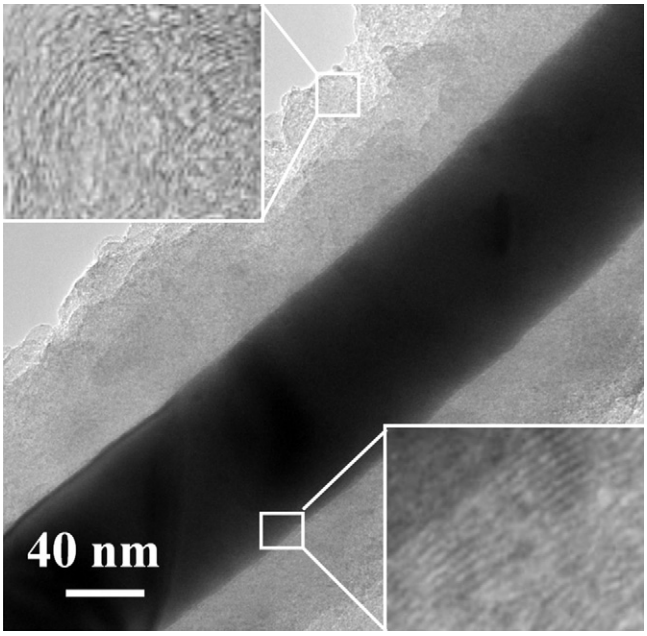

Fig. 2. HRTEM images of a HT nanostructure, presenting crystallinity of carbon at different locations in carbon nanotube. Left insert: Outer part of CNT; right insert: inner part of CNT.

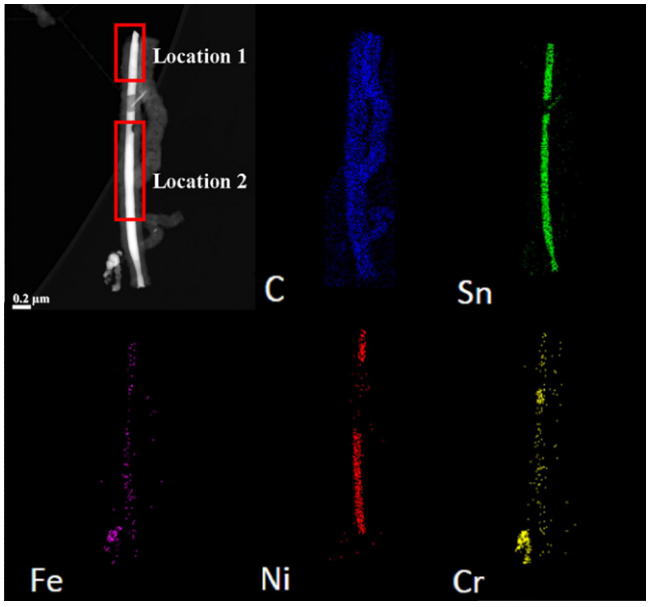

Fig. 3. STEM–EDS maps of a HT nanostructure on stainless steel, revealing the distribution of C, Sn, Fe, Ni and Cr along the core–shell structure.

of the inner metal nanowire is approximately 100 nm. The crystallinity of the carbon is not uniform in the CNT. The inner part of the CNT near the metal nanowires (Fig. 2, insert right) shows a relatively higher crystallinity than the part far from the metal nanowire (Fig. 2, insert left).

To investigate the effects of the substrate on the growth of the novel nanostructure, the composition of the HT nanostructure was characterized by STEM–EDS mapping technique (Fig. 3). The maps reveal that the outer shell is carbon and the inner core is not pure Sn nanowire but Sn alloy. The inner nanowire is mainly composed of Sn which alloyed with different metals including Fe, Ni and Cr along the growth direction of the nanowire. The starting material is pure Sn, and the substrate used in the synthesis is stainless steel 304 which contains various metals including Fe, Ni and Cr. Therefore, all the alloy elements (Fe, Ni, Cr) should originate from the stainless steel substrate.

To reveal the growth mechanism of HT nanostructure, the composition at different locations along the alloy nanowire was investigated. At location 1, the concentration of the various metals is: Sn 60.0 at.%, Ni 35.5 at.%, Fe 1.5 at.% and Cr 3.0 at.%; at location 2, the concentration is: Sn 55.8 at.%, Ni 36.6 at.%, Fe 4.1 at.% and Cr 3.5 at.%. The results show that the composition is not uniform along the nanowire. Based on the above analysis, the growth mechanism of the HT nanostructure was proposed. After pre-treatment, metals like Ni, Fe and Cr were exposed at the surface of the stainless steel. At the beginning of the reaction, Sn powder was evaporated at the elevating temperature and transferred to the stainless steel. Sn precursors deposited on the surface of stainless steel, and absorbed the Ni, Fe and Cr which were from the stainless steel to form the initial nuclei acting as catalyst for the decomposition of C_2H_4 (Fig. 4a). Fe and Ni have been reported as the most effective catalysts to generate CNTs [28–31]. The growth of CNTs directed by Fe and Ni usually includes decomposition, absorption and precipitation of carbon at the catalysts [32,33]. Sn could be also used as catalyst to produce CNTs [34], but the catalytic effect is not quite as effective due to the low carbon solubility in Sn [15]. The high total concentration of Ni (35.5–36.6 at.%) and Fe (1.5–4.1 at.%) in the final products indicate that the catalytic effect dominated the growth of the CNTs in the HT core–shell structure. The growth of CNTs and metal nanowires happened simultaneously during the growth (Fig. 4b). C_2H_4 interacted

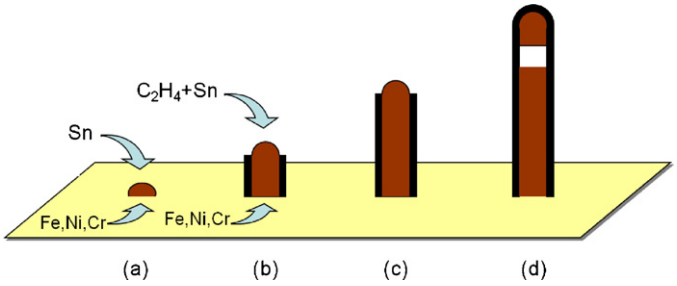

Fig. 4. Growth mechanism of the HT nanostructure on stainless steel. (a) Formation of initial alloyed nuclei; (b) simultaneous growth of the CNT and alloyed nanowire; (c) growth of the HT nanostructure; (d) final morphology of the HT nanostructure after solidification of the nanowire and associated cavity formation due to the volume change.

with the surface of the alloy nuclei and decomposed to provide carbon precursors. Carbon precursors then were absorbed by the alloy nuclei and subsequently precipitated at the surface to form CNTs. The precipitation of carbon from Sn and Fe/Ni was in a balanced process leading to a regular tube shape. Meanwhile, Sn precursors were absorbed at the top of the nuclei and joined the growth of the alloy nanowires. The growth of the unique core–shell structure was triggered and led to dense products (Fig. 4c). During the reaction, the continuous absorption of Sn would dilute the concentration of Ni, Fe and Cr at the top of nanowires. On the other hand, the involvement of Ni, Fe and Cr elements into the nanowires relied on the diffusion of the elements to the growth interface from the melted stainless steel substrates. Therefore, the concentration of Ni, Fe and Cr was lower at the top but higher at the bottom. The growth terminated when the experiment was stopped. The solid metal nanowires formed during the cooling process in which the small cavity formed inside the core–shell structure due to the volume change of metal from liquid to solid phase (Fig. 4d).

Different from the HT nanostructure, many small pores form inside the PF nanostructure, along the axis of the fibers (Fig. 5). The fibers have a very rough surface and metal particles are found sporadically embedded in the pores. The HRTEM images (Fig. 5 insert)

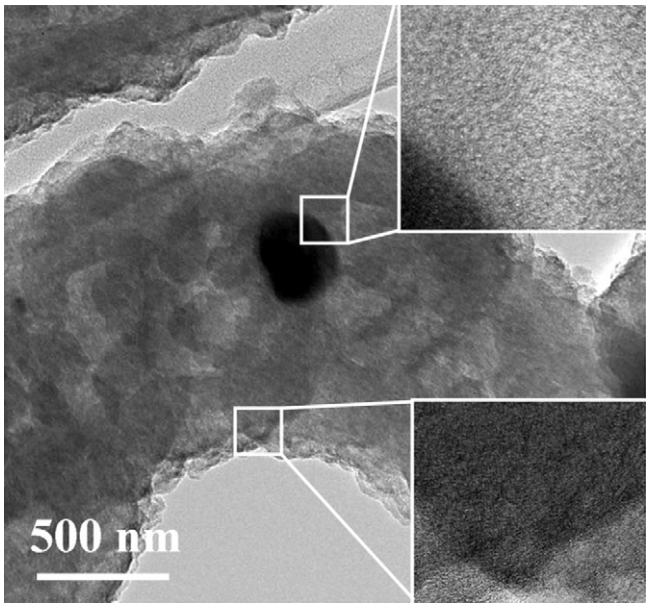

Fig. 5. HRTEM images of a PF nanostructure, presenting crystallinity of carbon at different locations in porous carbon fiber. Top inset: inner shell; bottom insert: outer shell.

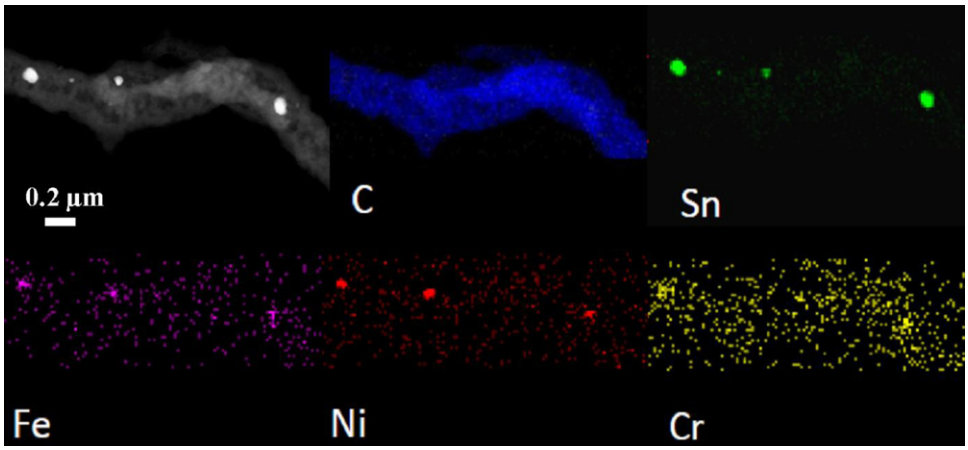

Fig. 6. STEM–EDS maps of a PF nanostructure on stainless steel, revealing the distribution of C, Sn, Fe, Ni and Cr along the fiber.

also reveal the low crystallinity of carbon near the metal particle and at the surface of carbon fiber.

Mapping results shown in Fig. 6 depict that the embedded particles are also alloy containing Sn 73.5 at.%, Ni 16.6 at.%, Fe 5.8 at.% and Cr 4.1 at.%, respectively. Fe, Ni and Cr which came from the stainless steel are not only contained in the metal particles, but also distribute along the carbon fibers. Based on the information, the growth mechanism of the PF nanostructure should be quite different from that of the HT nanostructure. After pre-treatment by HCl, the surface condition of the stainless steel was complicated and the composition was not homogeneous over the whole substrate. At the location which was rich in Fe and Ni, Fe and Ni were abundant in the initial nuclei and the growth was a catalytic process leading to HT nanostructure. While at the location where most of Fe and Ni were removed by HCl, there were less Fe and Ni but more Sn in the initial nuclei (Fig. 7a). The smaller amount of Fe and Ni could reduce the catalytic effect on the growth of CNTs. Then it was easy to form amorphous carbon during the growth. The composition of nuclei also leaded to an unbalanced process in terms of decomposition of carbon gas and precipitation of carbon due to the competitive effect between Sn and Fe/Ni. Meanwhile, fast deposition of amorphous carbon happened at this location. The initial alloy nuclei were quickly covered by thick carbon layers and

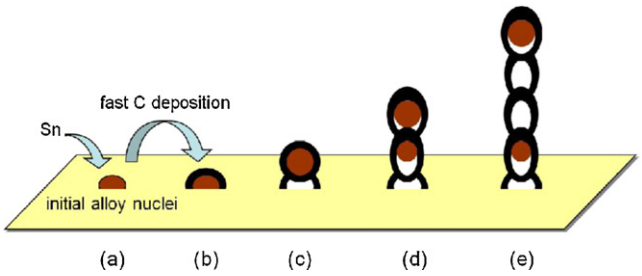

Fig. 7. Growth mechanism of the PF nanostructure on stainless steel. (a) formation of initial alloyed nuclei; (b) fast deposition of amorphous carbon at the initial alloyed nuclei; (c) growth of the PF nanostructure; (d) alloyed particles was periodically lifted up during growth while the small particle was trapped in the fiber; (e) final morphology of PF nanosturcture.

the supply of Sn precursors was not effective (Fig. 7b). Therefore, the unbalanced process happening at the nuclei and fast deposition of amorphous carbon resulted in the growth of porous fiber with irregular shape (Fig. 7c). During the growth, the initial nuclei were periodically lifted up, and some were trapped inside the fibers (Fig. 7d). Therefore, porous fibers containing alloy particles formed on the substrate (Fig. 7e).

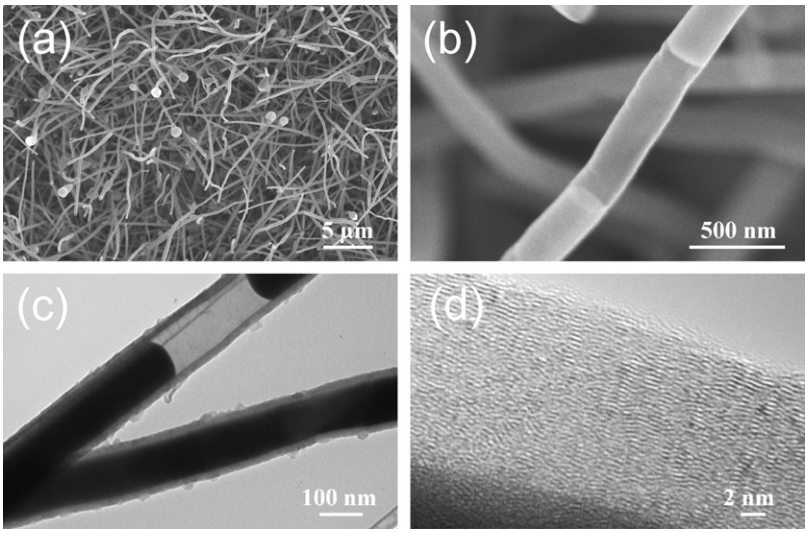

Fig. 8. SEM and HRTEM images of heterostructures growing on Cu. (a) dense 1D products on Cu; (b) hollow cell in the heterostructure; (c) HRTEM image of heterostructures; (d) CNT with relatively low crystallinity.

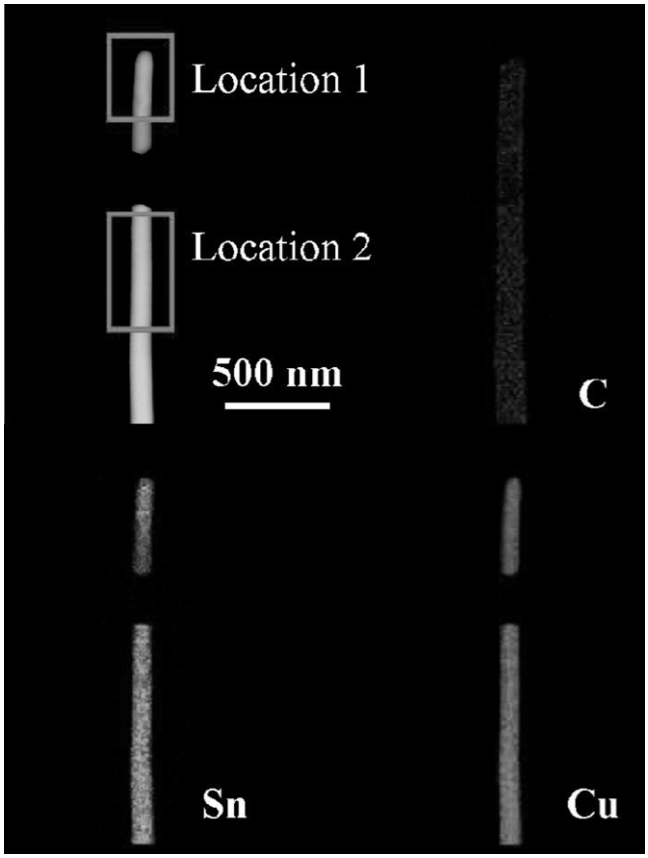

Fig. 9. STEM–EDS maps of a SnCu@CNT on Cu, revealing the distribution of C, Sn and Cu along the core–shell structure.

3.2. Cu substrate

On the other hand, the growth of heterostructures also happened on the Cu substrate. After reaction, very dense products were obtained on the Cu substrate (Fig. 8a). The products possess 1D nanowire-like morphology with a large range in diameter from 170 to 680 nm. Hollow cells are observed inside the nanostructure (Fig. 8b).

The TEM images in Fig. 8c and d reveal the further details of the products. The products possess a core–shell structure consisting of a solid core encapsulated inside a hollow tube (Fig. 8c). The hollow tubes are quite straight and long, with an average wall thickness of 23 nm. Both the inner and outer surfaces are smooth and clean. In Fig. 8d, layered structure can be clearly observed in the outer tube, owning to graphitic carbon. That indicates the hollow tube is CNT. However, the crystallinity of the CNT is relatively low.

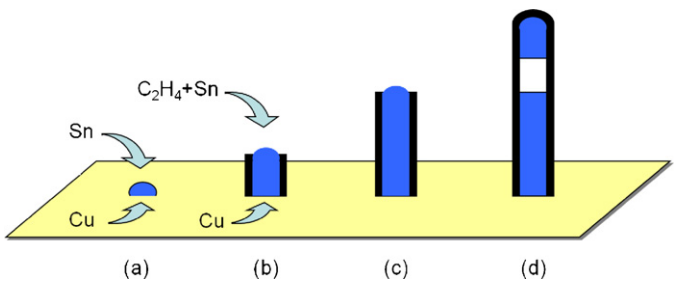

Fig. 10. Growth mechanism of the SnCu@CNT on Cu. (a) formation of initial alloyed nuclei; (b) simultaneous growth of CNT and alloyed nanowire; (c) growth of SnCu@CNTs; (d) final morphology of SnCu@CNTs after reaction with hollow cell inside structure.

To investigate the further details of the core–shell structure, mapping characterization was carried out and the results were shown in Fig. 9. The maps present the composition and distribution of the elements in the core–shell structure. The outer shell is CNT while the inner solid core is the SnCu alloy nanowire (SnCu@CNT). The atomic ratios of Cu and Sn in the nanowire are 83.9% and 16.1%, respectively. However, the distribution of the metals is not uniform along the nanowire's axis. At location 1, the composition is: Cu 85.6 at.% and Sn 14.4 at.%; at location 2, the composition is: Cu 82.7 at.% and Sn 17.3 at.%.

During the growth, Sn precursors were continuously absorbed in the vapor phase at the top of the alloy nuclei, while Cu was supplied by the substrate at the bottom. Therefore, the growth mechanism was very similar to that of the HT nanostructure on stainless steel. At the initial stage, Sn vapor was transferred to the Cu substrate. Cu could alloy with Sn at low temperatures [35], and formed small nuclei at the substrate surface (Fig. 10a). The small alloy nuclei which were rich in Cu, acted as the initial growing sites. Meanwhile, C_2H_4 was introduced into the reaction zone and decomposed at the surface of the alloy nuclei. The released carbon precursors were absorbed by alloy nuclei and joined the growth CNTs (Fig. 10b). Compared with Fe and Ni, Cu has an extremely low carbon solubility [36]. Therefore, the nuclei containing Sn and Cu presented low catalytic effect on the growth of CNTs which easily leaded to the formation of amorphous carbon. Because the growth was conducted in a balanced process of absorption and precipitation of carbon, the CNTs processed a regular 1D morphology in a straight tubular shape. Meanwhile, Sn was provided in vapor phase at the top part and Cu was supplied by the substrate at the bottom. The alloy nanowires formed simultaneously within CNTs and gradually grew into long one dimensional core–shell heteronanostructures (Fig. 10c). During the cooling process, the alloy became solid nanowires and hollow cells formed inside the core–shell structures (Fig. 10d).

4. Conclusions

SnM (M = (Fe, Ni, and Cr) or Cu) @ CNTs core–shell heterostructures were directly prepared on stainless steel and Cu substrates. The substrates can evidently affect the growth and morphology of the nanostructures. On the stainless steel substrate, the CNTs filled by Sn alloy nanowires and porous fibers filled by Sn alloy particles were observed; on the Cu substrate, SnCu alloy nanowires encapsulated in CNTs were found. Based on the analysis of the experimental results, the structures, morphology and features of the products are mainly determined by the surface composition deriving from the different types of substrates with pre-treatments. These heterostructures with unique features would be promising candidates as anode materials in Li-ion batteries applications. This method may be extended to grow other one dimensional heterostructures of carbon nanotubes encapsulated with alloy nanowires, in which low melting point metal is introduced by vaporized precursor while high melting point metal is fed by the substrate.

Acknowledgements

This research was supported by National Science and Engineering Research Council (NSERC), General Motors of Canada, Canada Research Chair (CRC) program, Canadian Foundation for Innovation (CFI), and the University of Western Ontario. The authors also appreciate the help from Mr. Fred Pearson at McMaster University.

References

[1] S. Iijima, Nature 354 (1991) 56.

[2] C. Liu, Y.Y. Fan, M. Liu, H.T. Cong, H.M. Cheng, M.S. Dresselhaus, Science 286 (1999) 1127.
[3] J. Kong, N.R. Franklin, C.W. Zhou, M.G. Chapline, S. Peng, K. Cho, H.J. Dai, Science 287 (2000) 622.
[4] P. Kim, C.M. Lieber, Science 286 (1999) 2148.
[5] Y. Wang, X. Jiang, Y. Xia, Journal of the American Chemical Society 125 (2003) 176.
[6] Y.J. Chen, Q.H. Li, Y.X. Liang, T.H. Wang, Q. Zhao, D.P. Yu, Applied Physics Letters 85 (2004) 5682.
[7] Y. Cheng, P. Xiong, L. Field, J.P. Zheng, R.S. Yang, Z.L. Wang, Applied Physics Letters 89 (2006) 093114.
[8] Q. Wan, E.N. Dattoli, W. Lu, Applied Physics Letters 90 (2007) 222107.
[9] S.G. Anasari, P. Boroojerdian, S.R. Sainkar, R.N. Karekar, R.C. Aiyer, S.K. Kulkarni, Thin Solid Films 295 (1997) 271.
[10] A. Kolmakov, Y.X. Zhang, G.S. Cheng, M. Moskovits, Advanced Materials 15 (2003) 997.
[11] X. Liang, Y. He, F. Liu, B. Wang, T. Zhong, B. Quan, G. Lu, Sensors and Actuators B 125 (2007) 544.
[12] W. Dazhi, W. Shulin, C. Jun, Z. Suyuan, L. Fangqing, Physical Review B 49 (1994) 282.
[13] S.S. Wong, J.D. Harper, P.T. Lansbury, C.M. Lieber, Journal of the American Chemical Society 120 (1998) 603.
[14] K.R. Prasad, N. Miura, Electrochemistry Communications 6 (2004) 849.
[15] R. Li, X. Sun, X. Zhou, M. Cai, X. Sun, Journal of Physical Chemistry C 111 (2007) 9130–9315.
[16] X. Ji, X. Huang, J. Liu, J. Jiang, X. Li, R. Ding, Y. Hu, F. Wu, Q. Li, Nanoscale Research Letters 5 (2010) 649.
[17] L. Pan, K. Lew, J.M. Redwing, E.C. Dickey, Journal of Crystal Growth 277 (2005) 428.
[18] M. Xin, Y. Chen, C. Jia, X. Zhang, Materials Letters 62 (2008) 2717.
[19] K. Kim, Y. Song, S. Chang, I. Kim, S. Kim, S.Y. Lee, Thin Solid Films 518 (2009) 1190.
[20] N. Singh, C. Yan, P.S. Lee, Sensors and Actuators B 150 (2010) 19.
[21] D.Q. Gao, D.S. Xue, Y. Xu, Z.J. Yan, Z.H. Zhang, Electrochimica Acta 54 (2009) 2392.
[22] W.M. Zhang, J.S. Hu, Y.G. Guo, S.F. Zheng, L.S. Zhong, W.G. Song, L.J. Wan, Advanced Materials 20 (2008) 1160.
[23] D. Deng, J.Y. Lee, Angewandte Chemie International Edition 48 (2009) 1660.
[24] M. Noh, Y. Kwon, H. Lee, J. Cho, Y. Kim, M.G. Kim, Chemistry of Materials 17 (2005) 1926.
[25] L. Jankovič, D. Gournis, P.N. Trikalitis, I. Arfaoui, T. Cren, P. Rudolf, M.H. Sage, T.T.M. Palstra, B. Kooi, J.D. Hosson, M.A. Karakassides, K. Dimos, A. Moukarika, T. Bakas, Nano Letters 6 (2006) 1131.
[26] S. Sun, G. Zhang, D. Geng, Y. Chen, M.N. Banis, R. Li, M. Cai, X. Sun, Chemistry: A European Journal 16 (2010) 829.
[27] R. Ragan, C.C. Ahn, H.A. Atwater, Applied Physics Letters 82 (2003) 3439.
[28] M.J. Bronikowski, Carbon 44 (2006) 2282.
[29] H. Sato, Y. Hori, K. Hata, K. Seko, H. Nakahara, Y. Saito, Journal of Applied Physics 100 (2006) 104321.
[30] Z. Li, J. Chen, X. Zhang, Y. Li, K.K. Fung, Carbon 40 (2002) 409.
[31] B.Q. Wei, Z.J. Zhang, P.M. Ajayan, G. Ramanath, Carbon 40 (2002) 47.
[32] S.B. Sinnott, R. Andrews, D. Qian, A.M. Rao, Z. Mao, E.C. Dickey, F. Derbyshire, Chemical Physics Letters 315 (1999) 25.
[33] A. Dupuis, Progress in Materials Science 50 (2005) 929.
[34] D. Yuan, L. Ding, H. Chu, Y. Feng, T.P. McNicholas, J. Liu, Nano Letters 8 (2008) 2576.
[35] M. Tan, B. Xiufang, X. Xiangying, Y.Z.G. Jing, S. Baoan, Physica B 387 (2007) 1.
[36] C.P. Deck, K. Vecchio, Carbon 44 (2006) 267.